AGU PUBLICATIONS

Geophysical Research Letters

RESEARCH LETTER
10.1002/2015GL065787

**Key Points:**
- Caprocks are intermediate wet or weakly water wet at typical storage conditions
- $CO_2$ wettability increases with pressure and thus depth
- Structural storage capacities are significantly lower than previously predicted

**Correspondence to:**
S. Iglauer,
stefan.iglauer@curtin.edu.au

**Citation:**
Iglauer, S., A. Z. Al-Yaseri, R. Rezaee, and M. Lebedev (2015), $CO_2$ wettability of caprocks: Implications for structural storage capacity and containment security, *Geophys. Res. Lett.*, *42*, 9279–9284, doi:10.1002/2015GL065787.

Received 13 AUG 2015
Accepted 16 SEP 2015
Accepted article online 23 SEP 2015
Published online 6 NOV 2015

©2015. American Geophysical Union. All Rights Reserved.

# $CO_2$ wettability of caprocks: Implications for structural storage capacity and containment security

**Stefan Iglauer[1], Ahmed Zarzor Al-Yaseri[1], Reza Rezaee[1], and Maxim Lebedev[2]**

[1]Department of Petroleum Engineering, Curtin University, Kensington, Western Australia, [2]Department of Exploration Geophysics, Curtin University, Kensington, Western Australia

**Abstract** Structural trapping, the most important $CO_2$ geostorage mechanism during the first decades of a sequestration project, hinges on the traditional assumption that the caprock is strongly water wet. However, this assumption has not yet been verified; and it is indeed not generally true as we demonstrate here. Instead, caprock can be weakly water wet or intermediate wet at typical storage conditions; and water wettability decreases with increasing pressure or temperature. Consequently, a lower storage capacity can be inferred for structural trapping in such cases.

## 1. Introduction

Carbon geosequestration (CGS) has been identified as a feasible technology to reduce anthropogenic $CO_2$ emissions and thus mitigate global warming [*Lackner*, 2003; *Intergovernmental Panel on Climate Change*, 2005; *Orr*, 2009]. In CGS, $CO_2$ is captured from large point-source emitters (e.g., coal-fired power stations), purified, compressed, and injected deep into the subsurface for storage. However, the $CO_2$ is buoyant as it has a lower density than the resident formation brine and thus flows upward. The primary sequestration mechanism during the first few decades of a storage project is structural trapping, where a caprock acts as a seal barrier to the $CO_2$ flow [*Armitage et al.*, 2013; *Wollenweber et al.*, 2010]. Caprock has a low permeability and associated with that small pores. Because of the small pore sizes (cp. equation (2) below), it is typically assumed that high capillary forces are created which prevent the $CO_2$ from entering the caprock [e.g., *Hesse et al.*, 2008]. However, a growing body of research papers suggests that pure minerals are not completely water wet [e.g. *Chiquet et al.*, 2007; *Broseta et al.*, 2012; *Farokhpoor et al.*, 2013; *Saraji et al.*, 2013; *Iglauer et al.*, 2014; *Sarmadivaleh et al.*, 2015; *Al-Yaseri et al.*, 2015a, 2015b; *Arif et al.*, 2016], and thus the capillary entry pressure for $CO_2$ can be dramatically reduced (and consequently also the structural trapping capacity).

However, despite these efforts, there is a serious lack of information in terms of real natural caprock, which is nevertheless most important. We thus tested several selected real caprock samples from a proposed storage site, and we demonstrate that the structural trapping capacity is significantly reduced at (high pressure) storage conditions.

## 2. Experimental Procedure

### 2.1. Caprock Samples

In order to constrain the uncertainty associated with structural trapping capacity predictions to an acceptable level, we selected eight caprock samples (Table 1) to experimentally evaluate their $CO_2$ wettability. These samples were retrieved from a proposed $CO_2$ storage site in New South Wales/Australia and thoroughly characterized [quantitative X-ray diffraction (XRD), total organic content (TOC), scanning electron microscopy-energy dispersive X-ray spectroscopy (SEM-EDS), thin section petrology, surface roughness, and mercury (Hg) intrusion measurements]. Most samples consisted mainly of quartz (~50–60 wt %), substantial amounts of clay (~20 wt % illite and chlorite), significant amounts of feldspar, and a few other minerals in low to medium concentrations, Table 1. An exception was sample 5, which had a high calcite content (47 wt %), and sample 3, which contained high amounts of illite (33 wt %). TOC ranged between 510 and 4400 mg/kg, typical for a deep saline aquifer. The SEM images show that clay (illite, illite-smectite, smectite, or kaolinite) filled the pore space and thus covered the surface of the grains. This observation is consistent with the EDS analysis, which mainly detected clay. Thin sections were analyzed for each sample at 40X and 100X magnification (Figure 1), and these results reflected the XRD and SEM-EDS measurements: the samples consisted mainly of quartz grains of varying size and angularity, with significant amounts of clays present. Several

**Table 1.** Geological and Chemical Properties of Caprock Samples Tested

| Sample | Depth (m) | TOC (mg/kg) | Chemical Composition[a] (wt %) | | Contact Angle (deg)[b] | Capillary Threshold Pressure (MPa)[c] | $CO_2$ Column Height (m)[d] |
|---|---|---|---|---|---|---|---|
| 1-Argillaceous siltstone | 1979.00 | 510 | Quartz | 54 | 47 | 0.82 | 241.3 |
| | | | Illite | 17 | | | |
| | | | Albite | 11 | | | |
| | | | Chlorite | 9 | | | |
| | | | K-feldspar (microcline) | 7 | | | |
| | | | Hematite | 2 | | | |
| 2-Calcareous sandstone | 1746.50 | 2600 | Quartz | 56 | 50 | n/a | n/a |
| | | | Ankerite | 12 | | | |
| | | | Calcite | 9 | | | |
| | | | Illite | 7 | | | |
| | | | Albite | 6 | | | |
| | | | Chlorite | 6 | | | |
| | | | Anhydrite | 4 | | | |
| 3-Shale | 1547.00 | 810 | Illite | 33 | 49 | 0.40 | 116.6 |
| | | | Quartz | 31 | | | |
| | | | Analcite | 15 | | | |
| | | | Albite | 9 | | | |
| | | | Chlorite | 8 | | | |
| | | | Hematite | 4 | | | |
| 4-Siltstone | 1506.00 | 2000 | Quartz | 46 | 44 | 1.35 | 392.8 |
| | | | Analcite | 20 | | | |
| | | | Chlorite | 12 | | | |
| | | | Illite | 12 | | | |
| | | | Albite | 9 | | | |
| | | | K-feldspar (microcline) | 1 | | | |
| 5-Calcareous siltstone | 1426.50 | 4400 | Calcite | 47 | 68 | 3.58 | 1043.5 |
| | | | Quartz | 27 | | | |
| | | | Albite | 8 | | | |
| | | | Ankerite | 5 | | | |
| | | | Illite | 5 | | | |
| | | | Analcite | 3 | | | |
| | | | Chlorite | 3 | | | |
| | | | K-feldspar (microcline) | 2 | | | |
| 6-Silty, argillaceous very fine grained sandstone | 1859.75 | 870 | Quartz | 64 | 48 | 0.25 | 74.5 |
| | | | Albite | 12 | | | |
| | | | Chlorite | 11 | | | |
| | | | Illite | 10 | | | |
| | | | Hematite | 2 | | | |
| | | | Calcite | 1 | | | |
| 7-Very fine grained clay bearing sandstone | 1865.06 | 1100 | Quartz | 62 | 50 | 0.24 | 69.5 |
| | | | Illite | 10 | | | |
| | | | Chlorite | 10 | | | |
| | | | Calcite | 8 | | | |
| | | | Albite | 5 | | | |
| | | | Anhydrite | 4 | | | |
| | | | Hematite | 1 | | | |
| 8-Very fine grained clay bearing sandstone | 1872 | 1600 | Quartz | 65 | 48 | 0.35 | 103.0 |
| | | | Albite | 13 | | | |
| | | | Illite | 10 | | | |
| | | | Chlorite | 10 | | | |
| | | | Hematite | 1 | | | |
| | | | Calcite | 1 | | | |

[a]Measured with a Bruker AXS XRD instrument.
[b]Water receding contact angle.
[c]Estimate for the conditions at 323 K and 15 MPa pore pressure using the *Boult et al.* [1997] method.
[d]Estimated from capillary threshold pressures using a capillary force-buoyancy force balance, equation (2).

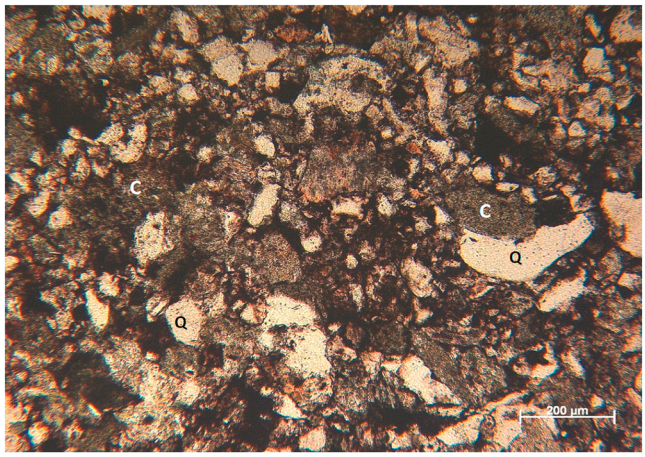


**Figure 1.** Selected thin section (clay = C and Q = quartz) image of caprock sample 6, 100X magnification.

samples also contained calcite and dolomite intergranular cements. Quartz overgrowth and intergranular clay formation were the dominant diagenetic features.

### 2.2. Experimental Tests

For the $CO_2$-wettability experiments, cuboid samples were cut with a high-speed diamond blade (to ~0.5 cm × 1 cm × 1 cm dimensions) and each sample was exposed to air plasma for 5 min to remove surface contaminants (note that this cleaning step is vital as otherwise the measurements are highly biased; contaminants are essentially all organic molecules present in the laboratory air; although their concentrations are low, they can significantly change the contact angles) [*Love et al.*, 2005; *Iglauer et al.*, 2014]. Importantly, the caprocks contained large amounts (when compared to molecular layers on a crystal surface) of organic material (TOC ranged from 510 to 4400 mg/kg, see above). During plasma cleaning, however, only the uppermost molecular layers of material are removed [*Alam et al.*, 2014]. As the caprock contained much more of the organic molecules, these naturally occurring organics were effectively not removed, and significantly higher contact angles (intermediate wetting) then for pure quartz crystals were measured, see below—thus the natural organic molecules in the caprock were preserved in the best possible way. Subsequently, the advancing ($\theta_a$) and receding ($\theta_r$) water contact angles were measured using the tilted plate method [*Lander et al.*, 1993] at storage conditions (15 MPa, 323 K, (20 wt % NaCl + 1 wt % KCl = 4.15 M ionic strength) brine). Note that prior to the measurements the surface topography of each sample was measured with an atomic force microscope (AFM, instrument model DSE 95–200), and the surface roughness was quantified as it can significantly influence $\theta$ and typically induces a difference between advancing and receding $\theta$ [*Marmur*, 2006] (Figure 2). The receding water contact angle $\theta_r$ corresponds to $CO_2$ entering the caprock and displacing brine and is thus most relevant to structural trapping capacity estimates (see equation (2) below). Root-mean-square (RMS) surface roughness ranged from 1100 to 1700 nm, which is fairly rough when compared to pure mineral substrates, with the exception of sample 1, which was very smooth (28 nm), similar to a geological single crystal mineral surface [*Sarmadivaleh et al.*, 2015]. The standard deviation of the measurements was determined as ±3° based on replicate measurements.

## 3. Results and Discussion

### 3.1. Contact Angles

All contact angles measured were quite similar, ~50°, except sample 5 had a higher contact angle (~70°). The hysteresis between $\theta_a$ and $\theta_r$ was small and insignificant despite significant surface roughness. We

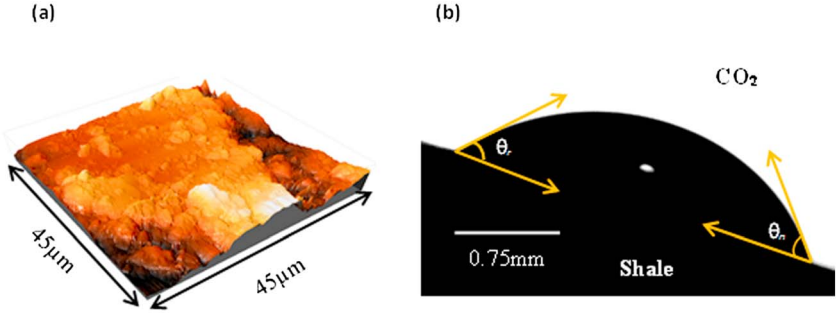


**Figure 2.** (a) Surface topography (measured with AFM, RMS surface roughness = 1100 nm, sample 7) and (b) brine drop on caprock sample with advancing ($\theta_a$) and receding ($\theta_r$) contact angles indicated.

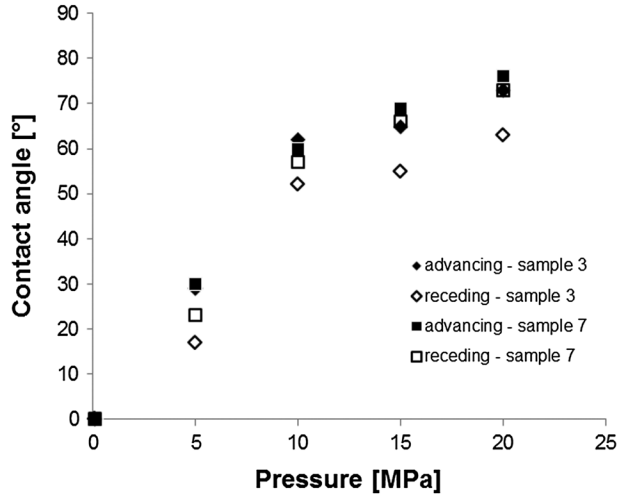


**Figure 3.** Advancing and receding water contact angles on caprock samples 3 and 7 as a function of pressure (measured at 343 K in (20 wt % NaCl + 1 wt % KCl) brine).

subsequently measured $\theta$ as a function of pressure at 343 K for samples 3 and 7, Figure 3, as pressure and temperature are expected to vary with storage depth [*Dake*, 1978]. Both caprock samples showed a similar $CO_2$-wettability behavior: $\theta$ increased dramatically with pressure and reached ~70° at 20 MPa. Such a trend has also been observed for clean silica surfaces [*Chiquet et al.*, 2007; *Jung and Wan*, 2012; *Saraji et al.*, 2013; *Iglauer et al.*, 2014; *Sarmadivaleh et al.*, 2015; *Al-Yaseri et al.*, 2015a, 2015b] and oil-wet surfaces [*Chi et al.*, 1988; *Dickson et al.*, 2006; *Li et al.*, 2007; *Yang et al.*, 2008]. Theoretical molecular dynamics predictions associate this effect with stronger $CO_2$-rock intermolecular interactions (which rise with pressure) [*Iglauer et al.*, 2012a]. An increase in temperature by 20 K (from 323 K to 343 K) increased $\theta$ by ~15°, a significant increase. Although this is consistent with what has been observed on quartz by some researchers [*Saraji et al.*, 2013; *Sarmadivaleh et al.*, 2015], it is inconsistent with *Wang et al.*'s [2013] and *Farokhpoor et al.*'s [2013] measurements where no temperature influence was observed and with *Iglauer et al.*'s [2012a] molecular dynamics predictions (note that in the molecular dynamics work, fully coordinated surfaces were investigated which are not fully representative of subsurface conditions). $\theta$ was significantly higher on the caprocks than on clean quartz [e.g., compare *Chiquet et al.*, 2007; *Farokhpoor et al.*, 2013; *Saraji et al.*, 2013; *Iglauer et al.*, 2014; *Sarmadivaleh et al.*, 2015; *Al-Yaseri et al.*, 2015a, 2015b] or calcite [*Farokhpoor et al.*, 2013], consistent with microcomputed tomography measurements [*Chaudhary et al.*, 2015]; this is probably due to the presence of organic material in the caprock. This conclusion is based on the fact that high water contact angles were measured on oil-wet substrates [e.g., *Dickson et al.*, 2006; *Li et al.*, 2007; *Espinoza and Santamarina*, 2010], compare the summary provided by *Iglauer et al.* [2015]. Hysteresis was small for sample 7, while a ~10° lower $\theta_r$ was measured for sample 3, which is probably due to its higher chemical heterogeneity as surface roughness of both samples were similar (1100 nm versus 1300 nm). The samples were thus weakly water wet or intermediate wet. This implies significantly lower structural trapping capacities [*Iglauer et al.*, 2015].

### 3.2. $CO_2$ Drainage Behavior

$CO_2$ drainage curves (Figure 4)—which characterize how $CO_2$ displaces brine from the caprock—were obtained by scaling mercury intrusion data (equation (1)):

$$P(CO_2) = \frac{P(Hg)\gamma(CO_2)\cos\theta(CO_2)}{\gamma(Hg)\cos\theta(Hg)}, \quad (1)$$

where $P(CO_2)$ is the $CO_2$ (drainage or capillary) pressure, $P(Hg)$ is the mercury intrusion pressure, $\gamma(CO_2)$ is the $CO_2$-brine interfacial tension (40 mN/m, taken from *Li et al.* [2012]), $\gamma(Hg)$ is the mercury-air interfacial tension (480 mN/m; *Tiab and Donaldson* [2004]), $\cos\theta(CO_2)$ is the

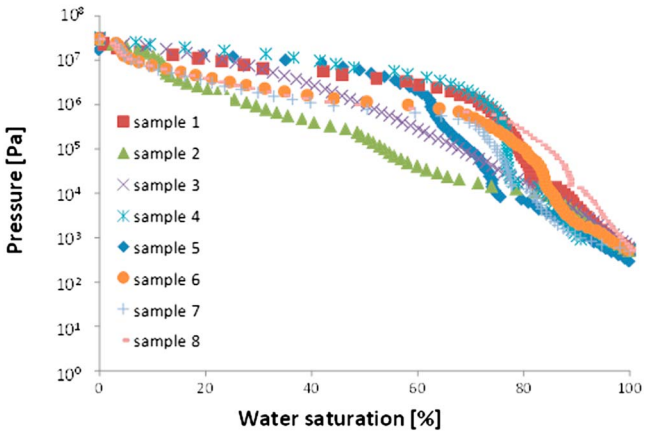


**Figure 4.** Supercritical $CO_2$ Primary Drainage Capillary Pressure Curves for the Caprock Samples Tested.

$CO_2$-brine-rock contact angle (measured here, cp. Figure 3), and cos$\theta$(Hg) is the mercury-air-rock contact angle (140°) [*Tiab and Donaldson*, 2004].

From these capillary pressure curves, the threshold pressures ($p_t$)—which correspond to the percolation threshold [*Thompson et al.*, 1987]—can be extracted. The threshold pressures extracted for the tested caprock samples varied substantially, between 0.2 and 3.6 MPa (Table 1), which is a significant variation and implies that a broad range of storage capacities can be expected (cp. equation (2) and Table 1). Please note that these are approximate estimates, as the extracted values depend on the method used to determine the threshold pressure (we used the method proposed by *Boult et al.* [1997], where a tangent through the drainage curve plateau is extrapolated to the pressure axis).

## 4. Conclusions and Implications

There is a serious lack of information regarding the $CO_2$ wettability of caprock despite its vital role for structural trapping capacity and containment security predictions. We thus measured $CO_2$ wettability of eight real natural caprock samples extracted from a proposed storage site in New South Wales in Australia. Our results demonstrate that the traditional assumption that a caprock for a brine-$CO_2$ system is completely water wet may not be true; instead, at reservoir conditions, the wettability of a caprock can reach up to 70°, implying a dramatically reduced sealing efficiency. Using the threshold pressures, equation (2) below [*Dake*, 1978], (capillary force-buoyancy force equilibrium) and assuming $\Delta\rho = 350\ \mathrm{kg/m^3}$ as a typical value for the fluid density difference [*Iglauer et al.*, 2015], we were able to predict maximum $CO_2$ column heights, which varied substantially, between ~70 and 1000 m. This implies that structural trapping is a feasible storage mechanism.

$$h = \frac{p_t}{\Delta\rho g} = \frac{2\gamma\cos\theta}{\Delta\rho g r}, \tag{2}$$

where $h$ is the $CO_2$ column height which can be permanently immobilized beneath a caprock, $p_t$ is the threshold pressure of the caprock, $\gamma$ is the $CO_2$-brine interfacial tension, $\theta$ is the brine-$CO_2$-rock contact angle, $\Delta\rho$ is the $CO_2$-brine density difference, $g$ is the gravitational constant, and $r$ is the average pore throat radius of the caprock material. While equation (2) assumes a fully connected $CO_2$ ganglion spanning the length $h$ as per Archimedes' principle, such connection, however, is difficult if not impossible to observe at the scale of tens to hundreds of meters. Hence, we must base our prediction on the experimental data and the best theory available. In this context, such large $CO_2$ clusters—which span essentially over the whole observed volume—have been measured with X-ray microcomputed tomography [e.g., *Iglauer et al.*, 2011; *Andrew et al.*, 2013] (note that "large" here means several millimeters as this is the limit for microtomography). Invasion percolation theory then predicts a cluster size distribution, which follows a power law (as confirmed by many experiments: *Iglauer et al.* [2010, 2011, 2012b, 2013], *Georgiadis et al.* [2013], *Andrews et al.* [2013], *Geistlinger and Mohammadian* [2015], etc.), which means that there are many small ganglia and only very few large ganglia. But (1) the large ganglia contribute most to the saturation, and (2) there are very large ganglia (although only very few of them) spanning through the whole volume, even if this volume is very large, and even for residual $CO_2$ clusters. Invasion percolation theory also predicts that the maximum $CO_2$ cluster volume $S_{max}$ (= largest ganglion size) scales as

$$S_{max} = S_{pores} n^D, \tag{3}$$

where $S_{pores}$ is the volume of a typical pore, $n$ is the number of pores across the sample, and $D$ is the fractal dimension (normally = 2.5) [*Wilkinson and Willemsen*, 1983; *Dias and Wilkinson*, 1986; *Iglauer et al.*, 2010].

In summary, importantly, structural trapping capacities are significantly reduced (when compared to completely water wet caprock) by a factor of $\cos\theta = \cos(50°) \approx 0.64$ at ~1500 m storage depth or $\cos(70°) \approx 0.34$ at ~2000 m storage depth. These data need to be incorporated into reservoir simulators in order to obtain reliable predictions and to guarantee containment security.

**Acknowledgments**
The authors wish to acknowledge financial assistance provided through Australian National Low Emissions Coal Research and Development (ANLEC R&D; grant number 3-0911-0155). ANLEC R&D is supported by Australian Coal Association Low Emissions Technology Limited and the Australian Government through the Clean Energy Initiative. The Iraqi Ministry of Higher Education and Scientific Research is thanked for providing financial support for Ahmed Zarzor Al-Yaseri. Furthermore, we would like to thank the New South Wales Government's Division of Resources and Energy for providing the caprock samples and associated petrophysical data and analyses, and the National Measurements Institute of Australia for conducting the TOC measurements on the caprock samples.

The Editor thanks Jan Vinogradov and an anonymous reviewer for their assistance in evaluating this paper.

## References

Alam, A. U., M. M. R. Howlader, and M. J. Deen (2014), The effects of oxygen plasma and humidity on surface roughness, water contact angle and hardness of silicon, silicon dioxide and glass, *J. Micromech. Microeng.*, *24*, 035010, doi:10.1088/0960-1317/24/3/035010.

Al-Yaseri, A., M. Sarmadivaleh, A. Saeedi, M. Lebedev, A. Barifcani, and S. Iglauer (2015a), $N_2$ + $CO_2$ + NaCl brine interfacial tensions and contact angles on quartz at CO2 storage site conditions in the Gippsland Basin, Victoria/Australia, *J. Petrol. Sci. Eng.*, *129*, 58–62.

Al-Yaseri, A., M. Lebedev, and S. Iglauer (2015b), Receding and advancing CO2-brine-quartz contact angles as a function of pressure, temperature, surface roughness and salinity, *J. Chem. Thermodyn.*, in press.
Andrew, M., B. Bijeljic, and M. J. Blunt (2013), Pore-scale imaging of geological carbon dioxide storage under in situ conditions, *Geophys. Res. Lett.*, *40*, 3915–3918, doi:10.1002/grl.50771.
Arif, M., A. Z. Al-Yaseri, M. Lebedev, A. Barifcani, and S. Iglauer (2016), Impact of pressure and temperature on $CO_2$-brine-mica contact angles and CO2-brine interfacial tension: Implications to carbon geo-sequestration, *J. Colloid Interface Sci.*, *462*, 208–215.
Armitage, P. J., D. R. Faulkner, and R. H. Worden (2013), Caprock corrosion, *Nat. Geosci.*, *6*, 79–80, doi:10.1038/ngeo1716.
Boult, P. J., P. N. Theologou, and J. Foden (1997), Capillary seals within the Eromanga Basin, Australia: Implications for exploration and production, in *Seals, Traps and the Petroleum System*, *AAPG Mem.*, vol. 67, edited by R. C. Surdam, pp. 143–167, AAPG, Tulsa, Okla.
Broseta, D., N. Tonnet, and V. Shah (2012), Are rocks still water-wet in the presence of dense $CO_2$ or $H_2S$?, *Geofluids*, *12*, 280–294.
Chaudhary, K., E. J. Guiltinan, M. Bayani Cardenas, J. A. Maisano, R. A. Ketcham, and P. C. Bennett (2015), Wettability measurement under high P-T conditions using X-ray imaging with application to the brine-supercritical $CO_2$ system, *Geochem. Geophys. Geosyst.*, doi:10.1002/2015GC005936, in press.
Chi, S.-M., B. I. Morsi, G. E. Klinzing, and S.-H. Chiang (1988), Study of interfacial properties in the liquid $CO_2$-water-coal system, *Energy Fuels*, *2*, 141–145.
Chiquet, P., D. Broseta, and S. Thibeau (2007), Wettability alteration of caprock minerals by carbon dioxide, *Geofluids*, *7*, 112–122.
Dake, L. P. (1978), *Fundamentals of Reservoir Engineering*, Elsevier, Amsterdam.
Dias, M. M., and D. Wilkinson (1986), Percolation with trapping, *J. Phys. A: Math. Gen.*, *19*, 3131–3146.
Dickson, J. L., G. Gupta, T. S. Horozov, B. P. Binks, and K. P. Johnston (2006), Wetting phenomena at the $CO_2$/water/glass interface, *Langmuir*, *22*(5), 2161–2170.
Espinoza, D. N., and J. C. Santamarina (2010), Water-$CO_2$-mineral systems: Interfacial tension, contact angle, and diffusion—Implications to $CO_2$ geological storage, *Water Resour. Res.*, *46*, W07537, doi:10.1029/2009WR008634.
Farokhpoor, R., B. J. A. Bjørkvik, E. Lindeberg, and O. Torsæter (2013), Wettability behaviour of $CO_2$ at storage conditions, *Int. J. Greenhouse Gas Control*, *12*, 18–25.
Geistlinger, H., and S. Mohammadian (2015), Capillary trapping mechanism in strongly water-wet systems: Comparison between experiment and percolation theory, *Adv. Water Resour.*, *79*, 35–50.
Georgiadis, A., S. Berg, A. Makurat, G. Maitland, and H. Ott (2013), Pore-scale micro-computed tomography imaging: Non-wetting-phase cluster-size distribution during drainage and imbibition, *Phys. Rev. E*, *88*, 033002.
Hesse, M. A., F. M. Orr, and H. A. Tchelepi (2008), Gravity currents with residual trapping, *J. Fluid Mech.*, *611*, 35–60, doi:10.1017/S002211200800219X.
Iglauer, S., S. Favretto, G. Spinelli, G. Schena, and M. J. Blunt (2010), X-ray tomography measurements of power-law cluster size distributions for the nonwetting phase in sandstones, *Phys. Rev. E*, *82*, 056315.
Iglauer, S., A. Paluszny, C. H. Pentland, and M. J. Blunt (2011), Residual $CO_2$ imaged with X-ray micro-tomography, *Geophys. Res. Lett.*, *38*, L21403, doi:10.1029/2011GL049680.
Iglauer, S., M. Mathew, and F. Bresme (2012a), Molecular dynamics computations of brine-$CO_2$ interfacial tensions and brine-$CO_2$-quartz contact angles and their effects on structural and residual trapping mechanisms in carbon geo-sequestration, *J. Colloid Interface Sci.*, *386*, 405–414.
Iglauer, S., M. A. Fernø, P. Shearing, and M. J. Blunt (2012b), Comparison of residual oil cluster size distribution, morphology and saturation in oil-wet and water-wet sandstone, *J. Colloid Interface Sci.*, *375*(1), 187–192.
Iglauer, S., A. Paluszny, and M. Blunt (2013), Simultaneous oil recovery and residual gas storage: A pore-level analysis using in-situ x-ray micro-tomography, *Fuel*, *1*, 1–11.
Iglauer, S., A. Hassan, M. Sarmadivaleh, K. Liu, and C. Pham (2014), Contamination of silica surfaces: Impact on water-$CO_2$-quartz and glass contact angle measurements, *Int. J. Greenhouse Gas Control*, *22*, 325–328.
Iglauer, S., C. H. Pentland, and A. Busch (2015), $CO_2$-wettability of seal and reservoir rocks and the implications for carbon geo-sequestration, *Water Resour. Res.*, *51*, 729–774, doi:10.1002/2014WR015553.
Intergovernmental Panel on Climate Change (2005), IPCC special report on carbon dioxide capture and storage, prepared by Working Group III of the Intergovernmental Panel on Climate Change, Cambridge Univ. Press.
Jung, J.-W., and J. Wan (2012), Supercritical $CO_2$ and ionic strength effects on wettability of silica surfaces: Equilibrium contact angle measurements, *Energy Fuels*, *26*, 6053–6059.
Lackner, K. S. (2003), Climate change. A guide to $CO_2$ sequestration, *Science*, *300*, 1677–1678, doi:10.1126/science.1079033.
Lander, L. M., L. M. Siewierski, W. J. Brittain, and E. A. Vogler (1993), A systematic comparison of contact angle methods, *Langmuir*, *9*, 2237–2239, doi:10.1021/la00032a055.
Li, X., E. Boek, G. C. Maitland, and J. P. M. Trusler (2012), Interfacial tension of (brines + $CO_2$): (0.864 NaCl + 0.136 KCl) at temperatures between (298 and 448) K, pressures between (2 and 50) MPa, and total molalities of (1 to 5) mol · kg-1, *J. Chem. Eng. Data*, *57*(4), 1078–1088, doi:10.1021/je201062r.
Li, Y., J. Q. Pham, K. P. Johnston, and P. F. Green (2007), Contact angle of water on polystyrene thin films: Effects of $CO_2$ environment and film thickness, *Langmuir*, *23*, 9785–9793.
Love, J. C., L. A. Estroff, J. K. Kriebel, R. G. Nuzzo, and G. M. Whitesides (2005), Self-assembled monolayers of thiolates on metals as a form of nanotechnology, *Chem. Rev.*, *105*, 1103–1169.
Marmur, A. (2006), Soft contact: Measurement and interpretation of contact angles, *Soft Matter*, *2*, 12–17, doi:10.1039/B514811C.
Orr, F. M. (2009), Onshore geologic storage of $CO_2$, *Science*, *325*, 1656–1658, doi:10.1126/science.1175677.
Saraji, S., L. Goual, M. Piri, and H. Plancher (2013), Wettability of supercritical carbon dioxide/water/quartz systems: Simultaneous measurement of contact angle and interfacial tension at reservoir conditions, *Langmuir*, *29*, 6856–6866.
Sarmadivaleh, M., A. Z. Al-Yaseri, and S. Iglauer (2015), Influence of temperature and pressure on quartz-water-$CO_2$ contact angle and $CO_2$-water interfacial tension, *J. Colloid Interface Sci.*, *441*, 59–64, doi:10.1016/j.jcis.2014.11.010.
Thompson, A. H., A. J. Katz, and R. A. Raschke (1987), Mercury injection in porous media: A resistance devil's staircase with percolation geometry, *Phys. Rev. Lett.*, *58*(1), 29–32, doi:10.1103/PhysRevLett.58.29.
Tiab, D., and E. C. Donaldson (2004), *Petrophysics*, Elsevier, Amsterdam.
Wang, S., Z. Tao, S. Persily, and A. F. Clarens (2013), $CO_2$ adhesion on hydrated mineral surfaces, *Environ. Sci. Technol.*, *47*(20), 11,858–11,865.
Wilkinson, D., and J. F. Willemsen (1983), Invasion percolation: A new form of percolation theory, *J. Phys. A: Math. Gen.*, *16*, 3365–3376.
Wollenweber, J., S. Alles, A. Busch, B. M. Krooss, H. Stanjek, and R. Littke (2010), Experimental investigation of the $CO_2$ sealing efficiency of caprocks, *Int. J. Greenhouse Gas Control*, *4*, 231–241, doi:10.1016/j.ijggc.2010.01.003.
Yang, D., Y. Gu, and P. Tontiwachwuthikul (2008), Wettability determination of the reservoir brine—Reservoir rock system with dissolution of $CO_2$ at high pressures and elevated temperatures, *Energy Fuels*, *22*(1), 504–509.